Geophysical Research Letters

RESEARCH LETTER
10.1029/2024GL110409

Looking for Subsurface Oceans Within the Moons of Uranus Using Librations and Gravity

D. J. Hemingway[1] and **F. Nimmo**[2]

[1]Institute for Geophysics, Jackson School of Geosciences, University of Texas at Austin, Austin, TX, USA, [2]Department of Earth and Planetary Sciences, University of California Santa Cruz, Santa Cruz, CA, USA

Key Points:

- Measuring physical libration amplitudes can be used to detect subsurface liquid water oceans within the Uranian moons
- Combining librations with gravity measurements can yield comprehensive constraints on the interiors of the Uranian moons
- Thick oceans are easier to detect but finding thin oceans may require libration amplitudes to be measured to within better than 10 m

Supporting Information:

Supporting Information may be found in the online version of this article.

Correspondence to:

D. J. Hemingway,
douglas.hemingway@utexas.edu

Citation:

Hemingway, D. J., & Nimmo, F. (2024). Looking for subsurface oceans within the moons of Uranus using librations and gravity. *Geophysical Research Letters*, *51*, e2024GL110409. https://doi.org/10.1029/2024GL110409

Received 23 MAY 2024
Accepted 3 SEP 2024

Author Contributions:

Conceptualization: D. J. Hemingway, F. Nimmo
Formal analysis: D. J. Hemingway
Investigation: D. J. Hemingway
Methodology: D. J. Hemingway
Software: D. J. Hemingway
Visualization: D. J. Hemingway
Writing – original draft: D. J. Hemingway
Writing – review & editing: F. Nimmo

Abstract Several of the icy moons in the Jupiter and Saturn systems appear to possess internal liquid water oceans. Our knowledge of the Uranian moons is more limited but a future tour of the system has the potential to detect subsurface oceans. Planning for this requires an understanding of how the moons' internal structures—with and without oceans—relate to observable quantities. Here, we show that the amplitude of forced physical librations could be diagnostic of the presence or absence of subsurface oceans within the Uranian moons. In the presence of a decoupling global ocean, ice shell libration amplitudes at Miranda, Ariel, and Umbriel will exceed 100 m if the shells are <30 km thick. The presence of oceans could also imply significant tidal heating within the last few hundred million years. Combining librations with the quadrupole gravity field could provide comprehensive constraints on the internal structures and histories of the Uranian moons.

Plain Language Summary Several of the icy moons in the Jupiter and Saturn systems appear to possess internal liquid water oceans. Our knowledge of the Uranian moons is more limited but a future tour of the Uranus system has the potential to detect subsurface oceans. Planning for this requires an understanding of how the moons' internal structures—with and without oceans—relate to observable quantities. Here, we show that certain aspects of their rotational states could be diagnostic of the presence or absence of internal liquid water oceans within several of the Uranian moons and that combining this with measurements of the gravity field could provide comprehensive constraints on the internal structures and histories of the Uranian moons.

1. Introduction

One of the most intriguing recent developments in the exploration of our solar system has been the detection of potentially habitable subsurface oceans inside several of the icy moons in the Jupiter and Saturn systems (Hemingway et al., 2018; Hussmann et al., 2006, 2015; F. Nimmo & Pappalardo, 2016; Spohn & Schubert, 2003). Much less is known about the moons of the Uranus system but they offer the possibility of additional ocean worlds with the potential to raise even more interesting questions. As the planetary science community begins preparation for a Uranus Flagship mission (Simon et al., 2021), it will be important to consider how the Uranian satellites could have evolved (Bierson & Nimmo, 2022; Castillo-Rogez et al., 2023; F. Nimmo, 2023; Ćuk et al., 2020) and how subsurface oceans could be detected within their interiors. Such results can help guide decisions about the tour design and the choices of instruments and their capabilities.

A variety of techniques have been used to detect the presence of internal liquid water oceans in the Jupiter and Saturn systems (F. Nimmo & Pappalardo, 2016). In some cases, geologic evidence or the appearance of recent or even active eruptions (i.e., at Enceladus; Porco et al., 2006) strongly suggest the presence of an internal liquid water ocean. Where the satellites are exposed to a time-varying magnetic field, as in the Jupiter system, magnetic induction signals have provided compelling evidence for electrically conductive layers (e.g., a salty liquid water ocean) at depth (Biersteker et al., 2023). Although this technique is expected to be effective in the Uranus system as well (Arridge & Eggington, 2021; Cochrane et al., 2021; Hussmann et al., 2006; Weiss et al., 2021), we will not focus on magnetic induction here.

Geodetic measurements can also be useful in multiple ways. Measurements of the shapes and gravitational fields of the satellites can be used to assess the compensation states of their ice shells, which may be suggestive of a subsurface ocean (e.g., Beuthe et al., 2016; Hemingway et al., 2018; D. J. Hemingway & Mittal, 2019; Iess et al., 2014; Zannoni et al., 2020; Čadek et al., 2016). Finally, measurements of the time-varying component of their shapes and/or gravitational fields (Iess et al., 2012; Moore, 2000), and/or characterization of their rotation states (i.e., obliquity and forced physical librations) (e.g., Baland et al., 2011; B. Bills & Nimmo, 2008; B. G. Bills

& Nimmo, 2011; Chen et al., 2014; Thomas et al., 2016; Van Hoolst et al., 2013, 2016) can provide key evidence for internal liquid water oceans because these can vary strongly as a function of internal structure and may be markedly different depending on whether or not the ice shell is mechanically decoupled from the deeper interior. The time variable part of the gravity signal—quantified by the tidal k_2 Love number—proved important for detecting a subsurface ocean at Titan (Goossens et al., 2024; Iess et al., 2012) but the small orbital eccentricities of the Uranian moons mean that their tidal response amplitudes are likely to be too small to measure without a dedicated orbiter. Titan's obliquity (the angle between its spin axis and orbit normal) was found to be a factor of ∼3 larger than what would be expected if the ice shell were physically coupled to the deeper interior (B. G. Bills & Nimmo, 2011; Chen et al., 2014), helping confirm the presence of an internal ocean there. Obliquity measurements in the Uranus system, especially at Oberon (Chen et al., 2014), similarly have the potential to reveal subsurface oceans, though we will not explore this possibility in the present work.

In this study, we will focus primarily on forced physical librations. All of the large satellites in the solar system are tidally locked with their parent body such that they experience a permanent tidal elongation. The resulting long axis of the satellite points approximately toward the parent body at all times but, because the satellites have elliptical orbits, alignment occurs only at pericenter and apocenter and the long axis is otherwise misaligned from the line connecting the satellite with the parent body (Murray & Dermott, 1999). This misalignment results in gravitational torques that act toward the east during half of the orbit (between pericenter and apocenter), and toward the west during the other half (from apocenter back to pericenter). The result is a small oscillation superimposed on the satellite's otherwise steady rotation rate. This is known as a forced physical libration and its amplitude can depend sensitively on the satellite's internal structure. For bodies whose ice shells behave rigidly and are physically decoupled from the deeper interior by a global subsurface ocean, the physical libration amplitude is a strong inverse function of shell thickness but is less sensitive to the deeper internal structure. We therefore also discuss the complementary measurement of the satellites' quadrupole gravity field and show that, taken together, these two measurements can provide comprehensive constraints on the internal structures of the large Uranian satellites. Though we will not directly model the thermal/orbital evolution of the satellites here (see e.g., Bierson & Nimmo, 2022; Castillo-Rogez et al., 2023; Ćuk et al., 2020), we will briefly discuss how constraining their present internal structures has implications for their thermal and orbital histories.

2. Methods

The methods necessary for our calculations are all available in the published literature but, for convenience, we summarize some of the most important equations in Appendix A. Both the libration amplitude and gravitational field calculations require a model of the satellite's internal structure. We represent each body as a series of concentric shells of uniform density, subject to the known radius and bulk density (Table S1 in Supporting Information S1). In our 'no-ocean' models, we specify only the densities of the two layers (icy mantle and rocky core) and we solve Equation A1 for the radius of the core. In our three layer models (ice, ocean, core), we specify all three layer densities and the thickness of the ice shell and solve Equation A1 for the radius of the core. None of the Uranian satellites are large enough for their hydrospheres to reach internal pressures at which high pressure ice phases need to be considered so this simple three-layer structure is sufficient for our purposes. We assume the bodies have relaxed to hydrostatic equilibrium and we calculate the expected hydrostatic figures for each layer following the methodology of Tricarico (2014). The resulting set of asymmetric concentric shells are used to calculate both the corresponding gravitational field asymmetries via Equation A3 and the libration amplitudes via Equation A11 or Equation A15, depending on whether or not a decoupling ocean is present. We account for the finite rigidity of the ice shells to allow for the possibility of deformation (we assume a Maxwell rheology) in response to the dynamical tidal forces, which can reduce libration amplitudes when the ice shells are thin, especially for the larger bodies (see Van Hoolst et al., 2013, and A2.2).

3. Results

For each of the five large Uranian satellites, we calculated the expected amplitude of forced physical librations under a variety of conditions (Figure 1). As a point of comparison, we also show results for Enceladus, where librations have been measured (Nadezhdina et al., 2016; Park et al., 2024; Thomas et al., 2016). Libration amplitude (measured in meters at the equator) increases with the body's radius and orbital eccentricity, and decreases with the body's bulk density and orbital period. As expected, the libration amplitudes of Titania and Oberon are significantly smaller than those of the three interior satellites, due primarily to their much larger semi-

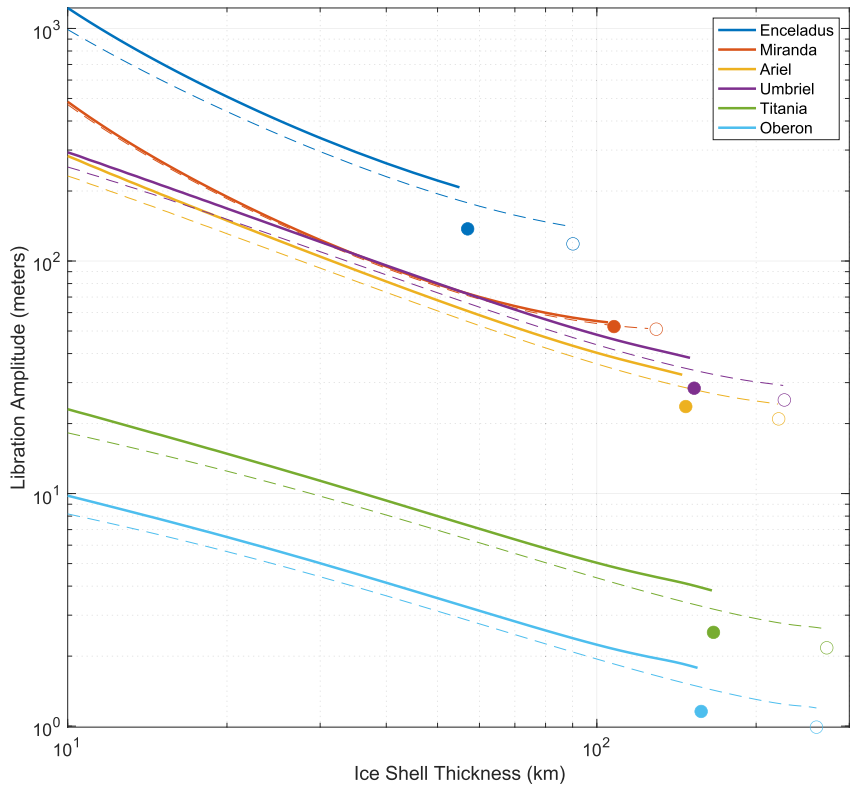

Figure 1. Amplitude of forced physical librations (at the equator) for several possible ocean worlds as a function of ice shell thickness. Circles represent libration amplitudes expected when no decoupling ocean is present. We assume $\rho_{ice} = 930$ kgm^{-3}, $\rho_{ocean} = 1{,}030$ kgm^{-3}, and either $\rho_{core} = 2{,}400$ kgm^{-3} (solid curves, filled circles) or $\rho_{core} = 3{,}500$ kgm^{-3} (dashed curves, open circles). Ice shell rigidity and viscosity are taken to be $\mu = 4$ GPa and $\eta = 10^{20}$ Pas (but see also Text S3 and Figure S6 in Supporting Information S1).

major axes. In spite of their different semi-major axes, the libration amplitudes of Miranda, Ariel, and Umbriel are similar due to opposing effects that approximately cancel: compared to Ariel, Miranda is closer to Uranus but smaller; compared to Ariel, Umbriel is farther from Uranus but has larger eccentricity (Figure S1 in Supporting Information S1). Enceladus is similar in size to Miranda but has a much larger eccentricity.

The circles in Figure 1 show the predicted libration amplitude in the absence of a decoupling ocean and are calculated via Equation A11. Results from *Cassini* imply core densities for Enceladus, Dione, and Titan in the range 2,300-2,500 kgm^{-3} (Durante et al., 2019; D. J. Hemingway & Mittal, 2019; Zannoni et al., 2020), suggestive of porous and/or hydrated silicate rock. Accordingly, we nominally assume $\rho_{core} = 2{,}400$ kgm^{-3}, though we also show results for $\rho_{core} = 3{,}500$ kgm^{-3} to illustrate the effect of varying core density up to the level of zero-porosity, non-hydrated chondritic rock. When a global subsurface ocean is present, the ice shell is mechanically decoupled from the rocky part of the interior and libration amplitude becomes a strong inverse function of shell thickness (Figure 1). We calculated libration amplitudes for each satellite considering ice shell thicknesses ranging from as small as 10 km up to the maximum thickness allowable given the bulk density constraints and the assumed density for the rocky core.

Our results for the 'no-ocean' case (circles in Figure 1) are smaller than those obtained by Comstock and Bills (2003) primarily because they use satellite eccentricities from Yoder (1995) whereas we use the values from Jacobson (2014), which are somewhat smaller. Since orbital eccentricities vary over time (e.g., Ćuk et al., 2020), the values from Jacobson (2014) are merely points of reference that correspond approximately to the present orbits, but note that varying orbital eccentricity has a straightforward, linear effect on libration amplitude. If we assume an infinitely rigid ice shell and calculate the libration amplitudes using Equation A13, our results (Figure S6 in Supporting Information S1) are similar to those of Park et al. (2020) (see their Figure 11), though they considered only the 'no-ocean' case and the case of a 20-km ocean with an ice shell thickness of either 20 km or

100 km. Libration amplitudes are slightly smaller when we allow for the possibility of elastic deformation, calculating libration amplitudes via Equation A15 (Figure 1).

Figure 1 illustrates that measurements of forced physical librations at the Uranian satellites could provide information about the presence of a decoupling global ocean as well as the thickness of the overlying ice shell. However, the libration amplitude is not sensitive to other aspects of the internal structure (e.g., ocean thickness, size and density of the rocky core). In contrast, the quadrupole gravity field, if it can be measured (see Castillo-Rogez et al., 2023), provides a constraint on the satellite's moment of inertia and thus the total thickness of the hydrosphere (ice shell plus ocean), but cannot easily distinguish between ice and water. To illustrate the utility of combining the two measurements, we simultaneously calculated the expected libration amplitude and quadrupole gravity field (we focus here on $C_{2,2}$) across a range of possible internal structures for each satellite. In each case, we assume a three-layer body consisting of an icy shell, a liquid water ocean, and a rocky core. We consider a wide range of ice shell thicknesses and rocky core densities and solve Equation A1 for the core radius and ocean thickness given the known total radius and bulk density of each body. The results are summarized in Figure 2, demonstrating that the combination of gravity plus libration observations simultaneously constrains shell thickness (teal contours), ocean thickness (dark blue contours), and core density (dashed gray contours); this is enough to also constrain the moment of inertia and core radius (not shown). In addition to the five Uranian moons, we show results for Enceladus with orange shading representing the observational constraints (Iess et al., 2014; Tajeddine et al., 2017; Thomas et al., 2016).

4. Discussion

Thomas et al. (2016) estimated the libration amplitude for Enceladus by reconstructing the rotation state based on optical tracking of surface features in a control point network across 7 years' worth of *Cassini* imagery. The resulting estimate was ∼530 m at the equator, with a 2-σ uncertainty of ∼60 m (a subsequent study by Park et al., 2024 obtained $\sim 400 \pm 40$ m, 3-σ). This strongly implies the presence of a subsurface ocean because even the low ends of these ranges are much larger than the value expected without a decoupling ocean (∼140 m). The precision of the libration measurement depends primarily on spacecraft/camera positioning and pointing errors, and the design of the tour/flybys (e.g., Park et al., 2020; Thomas et al., 2016). A large number of images from a variety of different viewing geometries helps to reduce uncertainties in the estimated libration amplitudes. In particular, it is important to obtain images that span a range of latitudes because the displacement of surface features due to physical librations will be largest at the equator and zero at the poles whereas displacements due to positioning/pointing errors will not vary with latitude in the same way (e.g., Hemingway et al., 2018). It is also essential to sample imagery from a variety of different true anomalies as the magnitude of displacements varies over the orbital period. Park et al. (2020) estimate that, with a camera designed for high-precision pointing, libration amplitudes could be constrained to within ∼1 m given enough measurements at sufficiently low altitudes (e.g., for the Enceladus example shown in their Figure 16, ∼10 measurements below 100 km altitude or ∼100 below 300 km). In that case, subsurface oceans should be detectable via librations under most conditions. We do not, however, take it for granted that such measurement precision will be easy to achieve (see Simon et al., 2021) and so we consider a wider range of possible uncertainties here.

From Figure 1, it is clear that the measurement precision required to detect a subsurface ocean depends on the shell and ocean thicknesses. For example, assuming $\rho_{\text{core}} = 2{,}400\ \text{kgm}^{-3}$, if Ariel has an ice shell thickness of 20 km (and therefore an ocean thickness of ∼140 km), the libration amplitude would be ∼150 m and 20 m of libration amplitude uncertainty would translate to just ∼2 km of uncertainty in the shell thickness estimate (Figure 1, S2 in Supporting Information S1). However, if the shell thickness is 120 km (ocean thickness is ∼30 km), the libration amplitude would be ∼36 m and 20 m of uncertainty would make a definitive ocean detection impossible since the 'no-ocean' value is ∼24 m. In other words, whereas a thick ocean is readily detectable, the case of a thin ocean may be indistinguishable from the no-ocean case unless libration amplitudes can be estimated with high precision (Figures S2, S3 in Supporting Information S1). Because the measurement precision required to distinguish between different internal structure models varies as a function of ice shell and ocean thickness, and is different for different bodies, it is impossible to provide a single number to target for measurement precision. Nevertheless, as a point of reference, for an ice shell thickness of 40 km, each 10 m of libration amplitude uncertainty translates to ∼5 km of ice/ocean thickness uncertainty for bodies like Miranda, Ariel, and Umbriel. For

10.1029/2024GL110409

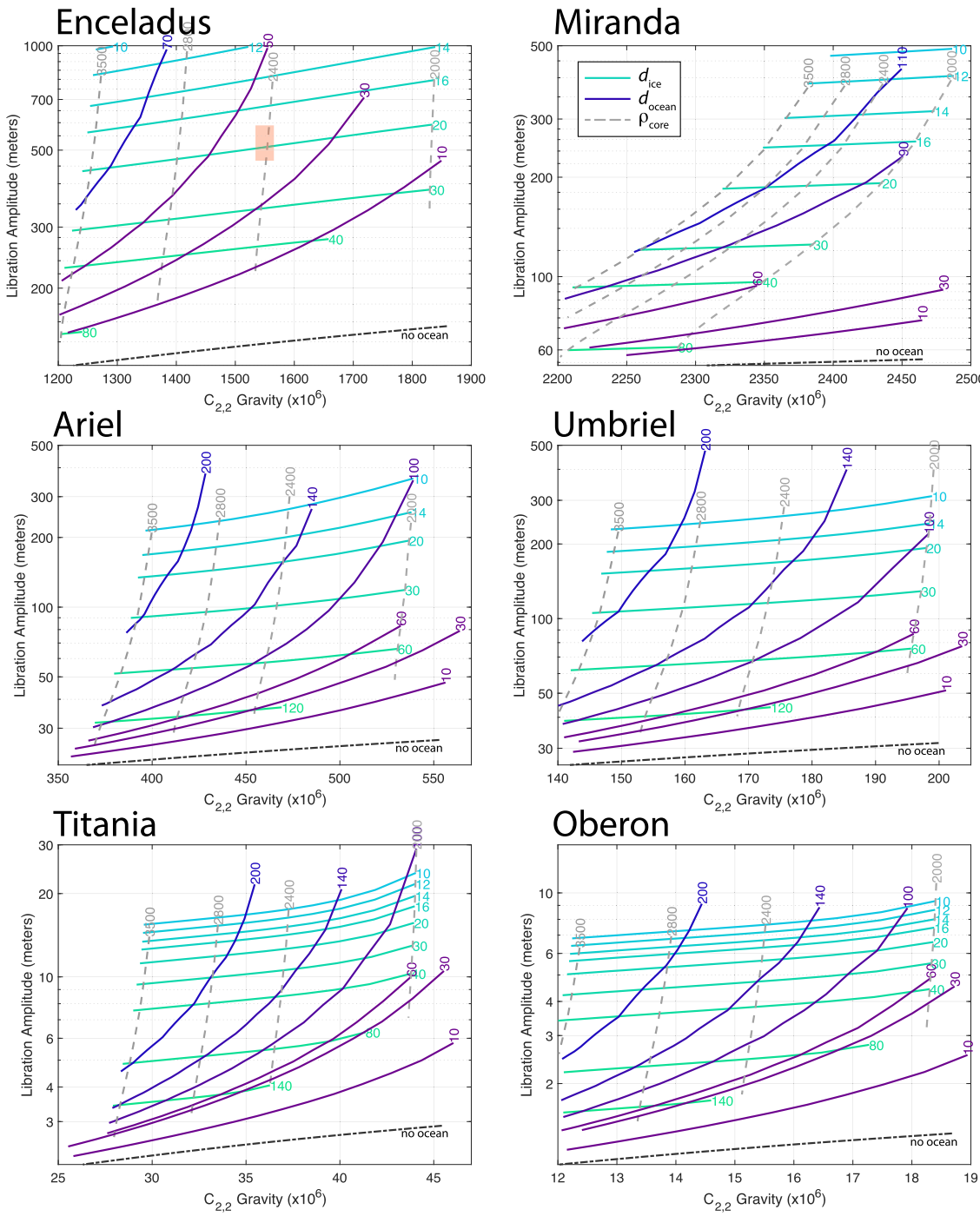

Figure 2. Contours show the implied thicknesses of the ice shell (teal) and ocean (dark blue), and the corresponding core density (dashed gray) as a function of libration amplitude (measured at the equator) and $C_{2,2}$ gravity (in units of dimensionless potential) for Enceladus and the five large Uranian moons. We assume $\rho_{\text{ice}} = 930\,\text{kgm}^{-3}$ and $\rho_{\text{ocean}} = 1{,}030\,\text{kgm}^{-3}$. Black dash-dotted lines show expectations without oceans. Ice shell rigidity and viscosity are taken to be $\mu = 4$ GPa and $\eta = 10^{20}$ Pas (but see also Text S3 and Figure S7 in Supporting Information S1). For Enceladus, orange shading marks the observational constraints.

Titania and Oberon, however, the corresponding figures are much larger: ∼60 km and ∼130 km, respectively. Hence, if the mission design allows for libration amplitude uncertainties comparable to those obtained by *Cassini* at Enceladus ($1\sigma \approx 20$ m at the equator), this method could be suited to detecting subsurface oceans at Miranda, Ariel, and Umbriel, provided they are not too thin (Text S1, Figures S2, S3 in Supporting Information S1). For

Titania and Oberon, however, libration amplitudes may be too small to measure with sufficient precision to detect subsurface oceans.

If the ice shells of the Uranian moons are thin enough to yield large libration amplitudes, significant internal heat production may be required. Conservatively assuming that all of the ice shells are conductive, we can compute, via Equation A17, the total conductive heat loss through the ice shells as a function of their thicknesses (Figure S4 in Supporting Information S1). As a point of reference, Enceladus's ice shell is estimated to be roughly 20 km thick on average, which corresponds to a total conductive heat loss of ∼30 GW (D. J. Hemingway & Mittal, 2019), assuming the ice-ocean interface is at a temperature of 273 K and that the thermal conductivity varies with temperature (and therefore depth) as $k = c/T$, where $c = 651\ \mathrm{Wm}^{-1}$ (Petrenko & Whitworth, 1999). In other words, roughly 30 GW of internal heat production is required within Enceladus in order to maintain its current ice shell thickness. The primary sources of internal heat production are tidal heating (most effective for bodies on short period eccentric orbits) and radiogenic heating (most effective for larger bodies with larger mass fractions of silicates). For Enceladus, radiogenic heating is negligible (Figure S5 in Supporting Information S1) so tidal heating must be the primary source of internal energy dissipation.

Given its similar size to Enceladus, Miranda has a similar relationship between shell thickness and required internal heat production, the biggest difference being the lower surface temperature of ∼60 K (vs. ∼75 K for Enceladus). Given the bulk density constraint and our assumed core density (2400 kgm^{-3}), the maximum permissible ice shell thickness for Miranda is ∼100 km (Figure 1), which corresponds to a total conductive heat loss of ∼4 GW (Figure S4 in Supporting Information S1) in the presence of a thin ocean. This is far in excess of radiogenic heat production (Figure S5 in Supporting Information S1) but if tidal heating were sufficiently intense, total internal heat production could exceed this value, leading to a thinner ice shell and a libration amplitude greater than ∼50 m (Figure 1). However, to yield a libration amplitude comparable to that of Enceladus (∼500 m at the equator), would require Miranda to have an ice shell thickness less than ∼10 km. To maintain such a small shell thickness would require ∼66 GW of internal heat production. For Ariel and Umbriel, which have roughly 6 times the surface area of Miranda, correspondingly larger internal heat production would be required to maintain the same shell thickness. For Titania and Oberon, the surface areas are a factor of ∼10 larger than Miranda's, requiring still greater internal heat production. Their larger volumes of rock yield more radiogenic heat (∼6 GW, Figure S5 in Supporting Information S1), but conductive heat loss is still greater, even for the thickest ice shells we considered (Figure S4 in Supporting Information S1).

A balanced heat budget may be easier to achieve under slightly different assumptions, however. For example, if we allow core densities greater than our nominal value ($\rho_{\mathrm{core}} > 2{,}400\ \mathrm{kgm}^{-3}$), the ice shells could be thicker than the thickest values shown in Figure S4 in Supporting Information S1, with heat loss being correspondingly smaller (though this will also reduce libration amplitudes, making them harder to measure). Furthermore, the above calculations assume pure water (with $T_{\mathrm{melt}} = 273$ K) and do not consider porosity. Heat loss could be somewhat more limited if the oceans are very cold. If melting occurs at the ammonia-water eutectic (176 K), for example, heat loss could be up to 30% smaller than the numbers calculated above and shown in Figure S4 in Supporting Information S1. Heat loss could also be reduced if thermal conductivity is less than what we assumed (section A3). For example, Bierson and Nimmo (2022) and Castillo-Rogez et al. (2023) both showed that some of the Uranian moons, particularly Titania and Oberon, could maintain long-lived internal oceans if the ice shells have very low thermal conductivity ($<3\ \mathrm{Wm}^{-1}\mathrm{K}^{-1}$), perhaps due to high porosity.

On the other hand, the heat budgets need not be balanced today. The presence of a subsurface ocean may instead be the fingerprint of a past epoch of efficient tidal heating, for example, when a larger orbital eccentricity was maintained by resonances between the satellites (Peterson et al., 2015; Ćuk et al., 2020). Without efficient tidal heating at present, any extant oceans may be in the process of freezing today. In that case, the current ice shell thickness could be used to approximately constrain how recently the ocean began freezing. Roughly speaking, assuming conductive cooling, the freezing timescale is related to thermal diffusion through the ice and can be approximated as $\tau \approx d^2/\kappa$, with $\kappa \approx 10^{-6}\mathrm{m}^2\mathrm{s}^{-1}$. This suggests that, in the absence of internal heat production, a 10 km thick ice shell could not have been freezing for more than ∼3 million years while a 100 km thick ice shell could not have been freezing for more than ∼300 million years (see also Castillo-Rogez et al., 2023). Hence, if librations reveal the presence of an internal ocean and yield an estimate of the ice shell's thickness, we can roughly constrain how recently tidal heating must have been operating—subject to assumptions about ocean chemistry and the thermal conductivity of the ice. The (past or present) efficacy of tidal heating within the interiors of the

Uranian satellites is difficult to determine but geologic evidence suggests that Miranda and Ariel experienced high surface heat flow at some point in their histories (Beddingfield et al., 2015, 2022a, 2022b; Bland et al., 2023; Pappalardo et al., 1997; Peterson et al., 2015). The energy available for tidal heating is related to the orbital evolution of the satellites and ultimately depends on the degree of dissipation (Q) within the interior of Uranus (F. Nimmo, 2023), which is not yet well determined. If the effective Q of Uranus is sufficiently low, a previous episode of tidal heating could have been enough to support liquid water oceans within the Uranian satellites (Castillo-Rogez et al., 2023; F. Nimmo, 2023).

5. Conclusions

We have shown that measurement of the forced physical libration amplitudes of the large Uranain satellites has the potential to reveal the presence of subsurface liquid water oceans within their interiors (Figure 1). We have shown that combined measurements of the libration amplitude and the quadrupole gravitational field can be used to simultaneously constrain the ice shell thickness, ocean thickness, and the size and density of the rocky core (Figure 2). For Miranda, Ariel, and Umbriel, libration amplitudes will exceed 100 m at the equator if the ice shells are less than 30 km thick. If libration amplitudes can be constrained to within a few tens of meters, subsurface oceans could be detected as long as they are not too thin (Figures 1 and 2, S2, S3 in Supporting Information S1). Oceans less than 40 km thick, however, may be difficult to detect unless libration amplitudes can be measured to within better than 10 m. For Titania and Oberon, libration amplitudes are likely less than 20 m, even if the ice shells are very thin, and so may be more challenging to measure.

We discussed the importance of constraining ice shell thickness and how it relates to the energy budgets of ocean worlds. If the ice shells are very thin, significant tidal heating would be required to keep the oceans from freezing (Figure S4 in Supporting Information S1) unless the ice shells have very low thermal conductivity and/or the ocean melting temperatures are significantly depressed (e.g., Bierson & Nimmo, 2022; Castillo-Rogez et al., 2023). Alternatively, the oceans could be in the process of freezing today. In that case, the current ice shell thickness could be used to determine roughly how recently tidal heating must have been effective—likely within the last few hundred million years for the cases we considered.

If flyby geometries and instrumentation can be selected to permit sufficiently precise measurements of libration amplitudes and the quadrupole gravitational field (Figures 1 and 2), a future tour of the Uranus system has the potential to reveal the presence of subsurface liquid water oceans and to help constrain the internal structures, energy budgets, and thermal/orbital evolution of the Uranian moons.

Appendix A: Detailed Methods

A1. Shape, Gravity, Internal Structure

Both the libration amplitude and gravitational field calculations require a model of the satellite's internal structure. We represent each body as a series of concentric shells of uniform density, subject to the known radius and bulk density (Table S1 in Supporting Information S1). The bulk density, $\bar{\rho}$, is related to the layer densities and radii by

$$\bar{\rho} = \sum_i \Delta\rho_i \left(\frac{R_i}{R}\right)^3 \tag{A1}$$

where R is the known outer radius, R_i is the mean radius of layer i, and $\Delta\rho_i$ is the density contrast between layer i and the layer above it. The mean moment of inertia, or moment of interia factor, is given by

$$\frac{I}{MR^2} = \frac{2}{5}\sum_i \frac{\Delta\rho_i}{\bar{\rho}}\left(\frac{R_i}{R}\right)^5 \tag{A2}$$

In our 'no-ocean' models, we specify only the densities of the two layers and we use the known total radius and bulk density to solve Equation A1 for the radius of the core. In our three layer models (ice, ocean, core), we specify all three layer densities and the thickness of the ice shell and again solve Equation A1 for the radius of the core.

We assume the bodies have relaxed to hydrostatic equilibrium, and we calculate the expected hydrostatic figures for each layer using the second order recursive method of Tricarico (2014) (see their Section 2.1.2). The degree-l and order-m gravitational field asymmetries arising from such a non-spherical multilayer body, and resolved at radius r, is given by

$$U_{lm}(r) = -\frac{4\pi G r}{2l+1}\sum_{i_{\text{below}}} \Delta\rho_i H_{ilm}\left(\frac{R_i}{r}\right)^{l+2} \tag{A3}$$

where H_{ilm} represents the shape of the i^{th} layer. The Tricarico (2014) approach to computing hydrostatic equilibrium figures involves approximating the layers as nested triaxial ellipsoids, with shapes represented in terms of polar and equatorial eccentricities, e_p and e_q, or by their semi-axes where

$$\begin{aligned} a &= \frac{R}{\left(\sqrt{1-e_p^2}\sqrt{1-e_q^2}\right)^{1/3}} \\ b &= a\sqrt{1-e_q^2} \\ c &= a\sqrt{1-e_p^2} \\ abc &= R^3 \end{aligned} \tag{A4}$$

which can, in turn, be related to the polar and equatorial flattenings

$$\begin{aligned} \alpha &= 1 - \frac{2c}{a+b} \\ \beta &= 1 - \frac{b}{a} \end{aligned} \tag{A5}$$

These triaxial ellipsoids can also be well approximated by degree-2 spherical harmonic expansions with only two non-zero coefficients

$$\begin{aligned} H_{2,0} &= \frac{1}{3}(2c - a - b) \\ H_{2,2} &= \frac{1}{6}(a - b) \end{aligned} \tag{A6}$$

For simplicity, we have not shown the subscript i in Equations A4–A6, but it should be understood that each layer has its own R, a, b, c, e_p, e_q, α, β, and H_{lm}.

A, B, and C are the principal moments of inertia (in general $A < B < C$ for synchronous satellites) and are given by

$$\begin{aligned} A &= \int \rho\left(y^2 + z^2\right) dV \\ B &= \int \rho\left(x^2 + z^2\right) dV \\ C &= \int \rho\left(x^2 + y^2\right) dV \end{aligned} \tag{A7}$$

where ρ is the density of a volume element dV at position x, y, z within the body. From the above, it can be shown that, for a body consisting of nested triaxial ellipsoids,

$$\frac{B-A}{C} = \frac{\sum_i \Delta\rho_i\left(a_i^2 - b_i^2\right) a_i b_i c_i}{\sum_i \Delta\rho_i\left(a_i^2 + b_i^2\right) a_i b_i c_i} \tag{A8}$$

which is the satellite's dynamical triaxiality (sometimes denoted Σ). Note that while we generally compute the gravity moments via Equation A3, it can also be shown that $C_{2,2} = \frac{B-A}{4MR^2}$.

A2. Forced Physical Libration Amplitude

A2.1. Without an Ocean

When no decoupling ocean is present, the ice shell and rocky core rotate together and the libration amplitude is given by (Murray & Dermott, 1999, p. 216)

$$\gamma = \frac{2e}{1-(n/\omega_0)^2} \tag{A9}$$

where e is the orbital eccentricity, $n = 2\pi/P$ is the satellite's mean motion, where P is the orbital period, and ω_0 is the free libration frequency given by (Comstock & Bills, 2003)

$$\omega_0 = n\sqrt{3\frac{B-A}{C}} \tag{A10}$$

where the satellite's dynamical triaxiality, $(B-A)/C$, is given by Equation A8. It follows that

$$\gamma = \frac{2e}{1-\frac{C}{3(B-A)}} = \frac{6e}{\left(3\frac{B-A}{C}-1\right)}\frac{B-A}{C} \tag{A11}$$

Because $B-A$ is much smaller than C, the libration amplitude is often approximated as

$$\gamma \approx -6e\frac{B-A}{C} \tag{A12}$$

A2.2. With a Decoupling Ocean

When the ice shell is mechanically decoupled from the rocky core by a liquid water ocean, the ice shell's response depends mainly on its thickness and rigidity (Goldreich & Mitchell, 2010; Van Hoolst et al., 2013). Although there is still gravitational coupling between the layers, this effect is minor compared to the mechanical coupling that occurs in the absence of an ocean. If the ice shell is sufficiently thick and the body is not too large (i.e., gravity is relatively weak), elastic forces in the ice shell dominate and the ice shell is effectively infinitely rigid. In this case, gravitational torques acting on the ice shell will cause it to oscillate in a way that depends mainly on its own moment of inertia (primarily a function of its thickness), with the libration amplitude given by (e.g., Thomas et al., 2016)

$$\gamma = \frac{2e\left[K_s\left(K_c + 2K_{int} - n^2C_c\right) + 2K_{int}K_c\right]}{C_sC_c\left(n^2-\omega_1^2\right)\left(n^2-\omega_2^2\right)} \tag{A13}$$

where ω_1 and ω_2 are the free libration frequencies (Van Hoolst et al., 2008). C_c and C_s are the separate polar moments of inertia for the rocky core and the icy shell, respectively, and are given by (e.g., Van Hoolst et al., 2008)

$$\begin{aligned} C_c &= \frac{8\pi}{15}\rho_c R_c^5\left(1+\frac{2}{3}\alpha_c\right) \\ C_s &= \frac{8\pi}{15}\rho_s\left[R_s^5\left(1+\frac{2}{3}\alpha_s\right) - R_o^5\left(1+\frac{2}{3}\alpha_o\right)\right] \end{aligned} \tag{A14}$$

where we use the subscripts s, o, and c for the shell, ocean, and core, respectively, and where the flattenings, α, are given by Equation A5. Finally, K_c and K_s are the amplitudes of the effective torques applied by the parent body on

the satellite's rocky core and icy shell, respectively, and K_{int} is the amplitude of the torque applied on the ice shell by the rest of the interior.

Equation A13 is a good approximation for Enceladus, Miranda, Ariel, and Umbriel, since elastic forces will dominate unless the ice shell is very thin (see Text S3 and Figures S6–S7 in Supporting Information S1). On the other hand, if the ice shell is thin and the body is large (i.e., gravity is strong), elastic stresses within the ice shell will be overcome by gravitational forces and the ice shell will deform in response to the changing tidal potential. To allow for this possibility, we in general follow the approach of Van Hoolst et al. (2013), computing the shell's libration amplitude using their equation (62)

$$\gamma = \frac{4e\left(K_3K_5 - K_2K_6 - n^2K_3C_{\text{c}}\right)}{C_{\text{c}}C_{\text{s}}\left(n^2 - \sigma_1^2\right)\left(n^2 - \sigma_2^2\right)} \tag{A15}$$

where the free frequencies σ_1 and σ_2 are given by Van Hoolst et al. (2013) equation (64). The K_1-K_6 terms, given by their equations (47)–(52), are related to the various torques that drive the physical librations. These include the external torques applied by the parent body on each of the satellite's layers (shell, ocean, and core), as well as the internal torques of each layer acting on the others.

Although we are assuming hydrostatic equilibrium (see A1), some non-hydrostatic topography is possible, especially for the smaller bodies. This can influence the torques by affecting the layers' moment of inertia differences, $(B - A)$. However, even in the case of Enceladus, where we have good constraints on the topography and have reason to believe there are large, non-hydrostatic lateral shell thickness variations (e.g., D. J. Hemingway & Mittal, 2019), the non-hydrostatic effects reduce the libration amplitude by just $\sim$6% assuming the mean ice shell thickness is 21 km; the effects are even smaller for larger shell thicknesses and/or larger bodies.

The Van Hoolst et al. (2013) formulation accounts for elastic deformation of the layers by calculating the dynamical Love numbers for each layer, given by (see their equation 24)

$$\begin{aligned} k_{2,\text{s}} &= \frac{4\pi G\rho_{\text{s}}}{5R^3}\left(R_{\text{s}}^4 y_{\text{s}} - R_{\text{o}}^4 y_{\text{o}}\right) \\ k_{2,\text{ot}} &= \frac{4\pi G\rho_{\text{o}}}{5R^3}\left(R_{\text{o}}^4 y_{\text{o}}\right) \\ k_{2,\text{ob}} &= \frac{4\pi G\rho_{\text{o}}}{5R^3}\left(-R_{\text{c}}^4 y_{\text{c}}\right) \\ k_{2,\text{c}} &= \frac{4\pi G\rho_{\text{c}}}{5R^3}\left(R_{\text{c}}^4 y_{\text{c}}\right) \end{aligned} \tag{A16}$$

which appear in some of the expressions for the torque amplitudes (Van Hoolst et al., 2013 equations 39–41, 54–57), along with the fluid Love numbers for each layer (see their eq. 25). In Equation A16, the effects of the ocean are divided into their top and bottom parts (*ot* and *ob*) because the top of the ocean follows the shape of the base of the ice shell while the bottom of the ocean follows the shape of the rocky core. R_{s}, R_{o}, and R_{c} are the mean radii of the shell, ocean, and rocky core, respectively, and y_{s}, y_{o}, and y_{c} are the radial displacements that arise at each of those radii in response to the changing tidal potential. We compute these radial displacements following the approach described by Roberts and Nimmo (2008) (see their eqs. 3–4, and Appendix A; we benchmarked our calculations against those of Roberts & Nimmo, 2008; Shao & Nimmo, 2022). This approach involves using a propagator matrix technique (e.g., Sabadini et al., 2016) to solve for the radial functions and approximating the inviscid ocean as a low-rigidity, low-viscosity material (we use $\mu = 10^6$ Pa and $\eta = 10^{11}$ Pas). We compute the complex rigidity of each layer assuming a Maxwell rheology (e.g., Tobie et al., 2005, equation 13).

A3. Heat Budget

Given an estimate of a satellite's mean ice shell thickness, d, we can estimate the minimum internal heat production required to balance the heat loss through the surface in order to maintain a subsurface liquid water ocean. We obtain a lower bound on surface heat flux by assuming a conductive ice shell, in which the thermal

conductivity varies with temperature (and therefore depth) as $k = c/T$, where $c = 651\ \mathrm{Wm}^{-1}$ is an experimentally derived constant (Petrenko & Whitworth, 1999). Conductive heat flux at the surface is then given by

$$F = \left(1 - \frac{d}{R}\right)\frac{c}{d}\ln\left(\frac{T_s}{T_b}\right) \tag{A17}$$

where T_s is the mean surface temperature, T_b is the temperature at the base of the ice shell (i.e., the melting temperature), and R is the mean radius of the body.

Data Availability Statement

All the data used in this research are freely available in the published literature. The estimated properties for the Uranian satellites (listed in Table S1 in Supporting Information S1) come from Jacobson (2014), P. C. Thomas (1988), and Widemann et al. (2009). For Enceladus, the shape comes from Tajeddine et al. (2017), the gravitational field comes from Iess et al. (2014), and the libration amplitude comes from Thomas et al. (2016) (but see also Park et al. (2024)).

Acknowledgments
This work was supported by the University of Texas Institute for Geophysics and the Jackson School of Geosciences at the University of Texas at Austin. We thank Tushar Mittal, Bob Jacobson, and Matt Clement for helpful discussions, and three anonymous reviewers for constructive suggestions that improved the manuscript.

References

Arridge, C. S., & Eggington, J. W. B. (2021). Electromagnetic induction in the icy satellites of Uranus. *Icarus*, *367*, 114562. https://doi.org/10.1016/j.icarus.2021.114562

Baland, R.-M., Van Hoolst, T., Yseboodt, M., & Karatekin, Ö. (2011). Titan's obliquity as evidence for a subsurface ocean? *Astronomy and Astrophysics*, *530*, A141. https://doi.org/10.1051/0004-6361/201116578

Beddingfield, C. B., Burr, D. M., & Emery, J. P. (2015). Fault geometries on Uranus' satellite Miranda: Implications for internal structure and heat flow. *Icarus*, *247*, 35–52. https://doi.org/10.1016/j.icarus.2014.09.048

Beddingfield, C. B., Cartwright, R. J., Leonard, E., Nordheim, T., & Scipioni, F. (2022). Ariel's elastic thicknesses and heat fluxes. *The Planetary Science Journal*, *3*(5), 106. https://doi.org/10.3847/PSJ/ac63d1

Beddingfield, C. B., Leonard, E., Cartwright, R. J., Elder, C., & Nordheim, T. A. (2022). High heat flux near Miranda's inverness corona consistent with a geologically recent heating event. *The Planetary Science Journal*, *3*(7), 174. https://doi.org/10.3847/PSJ/ac7be5

Beuthe, M., Rivoldini, A., & Trinh, A. (2016). Enceladus's and Dione's floating ice shells supported by minimum stress isostasy. *Geophysical Research Letters*, *43*(19). https://doi.org/10.1002/2016GL070650

Bierson, C. J., & Nimmo, F. (2022). A note on the possibility of subsurface oceans on the Uranian satellites. *Icarus*, *373*, 114776. https://doi.org/10.1016/j.icarus.2021.114776

Biersteker, J. B., Weiss, B. P., Cochrane, C. J., Harris, C. D. K., Jia, X., Khurana, K. K., et al. (2023). Revealing the interior structure of icy moons with a Bayesian approach to magnetic induction measurements. *The Planetary Science Journal*, *4*(4), 62. https://doi.org/10.3847/PSJ/acc331

Bills, B., & Nimmo, F. (2008). Forced obliquity and moments of inertia of Titan. *Icarus*, *196*(1), 293–297. https://doi.org/10.1016/j.icarus.2008.03.002

Bills, B. G., & Nimmo, F. (2011). Rotational dynamics and internal structure of Titan. *Icarus*, *214*(1), 351–355. https://doi.org/10.1016/j.icarus.2011.04.028

Bland, M. T., Beddingfield, C. B., Nordheim, T. A., Patthoff, D. A., & Vance, S. D. (2023). Constraints on the composition and thermal structure of Ariel's icy crust as inferred from its largest observed impact crater. *Icarus*, *395*, 115452. https://doi.org/10.1016/j.icarus.2023.115452

Čadek, O., Tobie, G., Van Hoolst, T., Massé, M., Choblet, G., Lefèvre, A., et al. (2016). Enceladus's internal ocean and ice shell constrained from Cassini gravity, shape, and libration data. *Geophysical Research Letters*, *43*(11), 5653–5660. https://doi.org/10.1002/2016GL068634

Castillo-Rogez, J., Weiss, B., Beddingfield, C., Biersteker, J., Cartwright, R., Goode, A., et al. (2023). Compositions and interior structures of the large moons of Uranus and implications for future spacecraft observations. *Journal of Geophysical Research: Planets*, *128*(1), e2022JE007432. https://doi.org/10.1029/2022JE007432

Chen, E. M. A., Nimmo, F., & Glatzmaier, G. A. (2014). Tidal heating in icy satellite oceans. *Icarus*, *229*, 11–30. https://doi.org/10.1016/j.icarus.2013.10.024

Cochrane, C. J., Vance, S. D., Nordheim, T. A., Styczinski, M. J., Masters, A., & Regoli, L. H. (2021). In search of subsurface oceans within the Uranian moons. *Journal of Geophysical Research: Planets*, *126*(12), e2021JE006956. https://doi.org/10.1029/2021JE006956

Comstock, R. L., & Bills, B. G. (2003). A solar system survey of forced librations in longitude. *Journal of Geophysical Research*, *108*(E9), 5100. https://doi.org/10.1029/2003JE002100

Ćuk, M., El Moutamid, M., & Tiscareno, M. S. (2020). Dynamical history of the Uranian system. *The Planetary Science Journal*, *1*(1), 22. https://doi.org/10.3847/PSJ/ab9748

Durante, D., Hemingway, D., Racioppa, P., Iess, L., & Stevenson, D. (2019). Titan's gravity field and interior structure after Cassini. *Icarus*, *326*, 123–132. https://doi.org/10.1016/j.icarus.2019.03.003

Goldreich, P. M., & Mitchell, J. L. (2010). Elastic ice shells of synchronous moons: Implications for cracks on Europa and non-synchronous rotation of Titan. *Icarus*, *209*(2), 631–638. https://doi.org/10.1016/j.icarus.2010.04.013

Goossens, S., van Noort, B., Mateo, A., Mazarico, E., & van der Wal, W. (2024). A low-density ocean inside Titan inferred from Cassini data. *Nature Astronomy*, *8*(7), 846–855. https://doi.org/10.1038/s41550-024-02253-4

Hemingway, D., Iess, L., Tadjeddine, R., & Tobie, G. (2018). The interior of Enceladus. In *Enceladus and the icy moons of Saturn*. The University of Arizona Press. https://doi.org/10.2458/azu_uapress_9780816537075-ch004

Hemingway, D. J., & Mittal, T. (2019). Enceladus's ice shell structure as a window on internal heat production. *Icarus*, *332*, 111–131. https://doi.org/10.1016/j.icarus.2019.03.011

Hussmann, H., Sohl, F., & Spohn, T. (2006). Subsurface Oceans and deep interiors of medium-sized outer planet satellites and large Trans-neptunian objects. *Icarus*, *185*(1), 258–273. https://doi.org/10.1016/j.icarus.2006.06.005

Hussmann, H., Sotin, C., & Lunine, J. I. (2015). Interiors and evolution of icy satellites. In *Treatise on Geophysics* (pp. 605–635). Elsevier. https://doi.org/10.1016/B978-0-444-53802-4.00178-0

Iess, L., Jacobson, R. A., Ducci, M., Stevenson, D. J., Lunine, J. I., Armstrong, J. W., et al. (2012). The tides of Titan. *Science*, *337*(6093), 457–459. https://doi.org/10.1126/science.1219631

Iess, L., Stevenson, D. J., Parisi, M., Hemingway, D., Jacobson, R. A., Lunine, J. I., et al. (2014). The gravity field and interior structure of Enceladus. *Science*, *344*(6179), 78–80. https://doi.org/10.1126/science.1250551

Jacobson, R. A. (2014). The orbits of the Uranian satellites and rings, the gravity field of the Uranian system, and the orientation of the Pole of Uranus. *The Astronomical Journal*, *148*(5), 76. https://doi.org/10.1088/0004-6256/148/5/76

Moore, W. (2000). The tidal response of Europa. *Icarus*, *147*(1), 317–319. https://doi.org/10.1006/icar.2000.6460

Murray, C. D., & Dermott, S. F. (1999). *Solar system dynamics*. Cambridge Univ. Press. Cambridge [u.a].

Nadezhdina, I. E., Zubarev, A. E., Brusnikin, E. S., & Oberst, J. (2016). A libration model for Enceladus based on geodetic control point network analysis. In *The international archives of the photogrammetry, remote sensing and spatial information sciences XLI-B4* (pp. 459–462). https://doi.org/10.5194/isprs-archives-XLI-B4-459-2016

Nimmo, F. (2023). Strong tidal dissipation at Uranus? *The Planetary Science Journal*, *4*(12), 241. https://doi.org/10.3847/PSJ/ad0cfb

Nimmo, F., & Pappalardo, R. T. (2016). Ocean worlds in the outer solar system. *Journal of Geophysical Research: Planets*, *121*(8), 1378–1399. https://doi.org/10.1002/2016JE005081

Pappalardo, R. T., Reynolds, S. J., & Greeley, R. (1997). Extensional tilt blocks on Miranda: Evidence for an upwelling origin of Arden Corona. *Journal of Geophysical Research*, *102*(E6), 13369–13379. https://doi.org/10.1029/97JE00802

Park, R. S., Mastrodemos, N., Jacobson, R. A., Berne, A., Vaughan, A. T., Hemingway, D. J., et al. (2024). The global shape, gravity field, and libration of Enceladus. *Journal of Geophysical Research: Planets*, *129*(1), e2023JE008054. https://doi.org/10.1029/2023JE008054

Park, R. S., Riedel, J. E., Ermakov, A. I., Roa, J., Castillo-Rogez, J., Davies, A. G., et al. (2020). Advanced pointing imaging camera (APIC) for planetary science and mission opportunities. *Planetary and Space Science*, *194*, 105095. https://doi.org/10.1016/j.pss.2020.105095

Peterson, G., Nimmo, F., & Schenk, P. (2015). Elastic thickness and heat flux estimates for the Uranian satellite Ariel. *Icarus*, *250*, 116–122. https://doi.org/10.1016/j.icarus.2014.11.007

Petrenko, V. F., & Whitworth, R. W. (1999). *Physics of ice* (p. 373). Oxford University Press.

Porco, C. C., Helfenstein, P., Thomas, P. C., Ingersoll, A. P., Wisdom, J., West, R., et al. (2006). Cassini observes the active south Pole of Enceladus. *Science*, *311*(5766), 1393–1401. https://doi.org/10.1126/science.1123013

Roberts, J. H., & Nimmo, F. (2008). Tidal heating and the long-term stability of a subsurface ocean on Enceladus. *Icarus*, *194*(2), 675–689. https://doi.org/10.1016/j.icarus.2007.11.010

Sabadini, R., Vermeersen, B., & Cambiotti, G. (2016). *Global dynamics of the earth: Applications of viscoelastic relaxation theory to solid-earth and planetary Geophysics. Dordrecht*: Springer . https://doi.org/10.1007/978-94-017-7552-6

Shao, W. D., & Nimmo, F. (2022). An investigation of libration heating and the thermal state of Enceladus's ice shell. *Icarus*, *373*, 114769. https://doi.org/10.1016/j.icarus.2021.114769

Simon, A., Nimmo, F., & Anderson, R. (2021). *Uranus orbiter and probe: Journey to an ice giant system*. NASA.

Spohn, T., & Schubert, G. (2003). Oceans in the icy Galilean satellites of Jupiter? *Icarus*, *161*(2), 456–467. https://doi.org/10.1016/S0019-1035(02)00048-9

Tajeddine, R., Soderlund, K. M., Thomas, P. C., Helfenstein, P., Hedman, M. M., Burns, J. A., & Schenk, P. M. (2017). True polar wander of Enceladus from topographic data. *Icarus*, *295*, 46–60. https://doi.org/10.1016/j.icarus.2017.04.019

Thomas, P. C. (1988). Radii, shapes, and topography of the satellites of Uranus from Limb coordinates. *Icarus*, *73*(3), 427–441. https://doi.org/10.1016/0019-1035(88)90054-1

Thomas, P. C., Tajeddine, R., Tiscareno, M., Burns, J., Joseph, J., Loredo, T., et al. (2016). Enceladus's measured physical libration requires a global subsurface ocean. *Icarus*, *264*, 37–47. https://doi.org/10.1016/j.icarus.2015.08.037

Tobie, G., Mocquet, A., & Sotin, C. (2005). Tidal dissipation within large icy satellites: Applications to Europa and Titan. *Icarus*, *177*(2), 534–549. https://doi.org/10.1016/j.icarus.2005.04.006

Tricarico, P. (2014). Multi-layer hydrostatic equilibrium of planets and synchronous moons: Theory and application to Ceres and to solar system moons. *The Astrophysical Journal*, *782*(2), 99. https://doi.org/10.1088/0004-637X/782/2/99

Van Hoolst, T., Baland, R.-M., & Trinh, A. (2013). On the librations and tides of large icy satellites. *Icarus*, *226*(1), 299–315. https://doi.org/10.1016/j.icarus.2013.05.036

Van Hoolst, T., Baland, R.-M., & Trinh, A. (2016). The diurnal libration and interior structure of Enceladus. *Icarus*, *277*, 311–318. https://doi.org/10.1016/j.icarus.2016.05.025

Van Hoolst, T., Rambaux, N., Karatekin, Ö., Dehant, V., & Rivoldini, A. (2008). The librations, shape, and icy shell of Europa. *Icarus*, *195*(1), 386–399. https://doi.org/10.1016/j.icarus.2007.12.011

Weiss, B. P., Biersteker, J. B., Colicci, V., Goode, A., Castillo-Rogez, J. C., Petropoulos, A. E., & Balint, T. S. (2021). Searching for subsurface oceans on the moons of Uranus using magnetic induction. *Geophysical Research Letters*, *48*(19), e2021GL094758. https://doi.org/10.1029/2021GL094758

Widemann, T., Sicardy, B., Dusser, R., Martinez, C., Beisker, W., Bredner, E., et al. (2009). Titania's radius and an upper limit on its atmosphere from the September 8, 2001 stellar occultation. *Icarus*, *199*(2), 458–476. https://doi.org/10.1016/j.icarus.2008.09.011

Yoder, C. F. (1995). Astrometric and geodetic properties of earth and the solar system. In: *AGU reference shelf*. Ed. by T. J. Ahrens. American Geophysical Union, (pp. 1–31). https://doi.org/10.1029/RF001p0001

Zannoni, M., Hemingway, D., Gomez Casajus, L., & Tortora, P. (2020). The gravity field and interior structure of Dione. *Icarus*, *345*, 113713. https://doi.org/10.1016/j.icarus.2020.113713